

Article

Motion-Induced Radiation Due to an Atom in the Presence of a Graphene Plane

César D. Fosco¹, Fernando C. Lombardo²  and Francisco D. Mazzitelli^{1,*}

¹ Centro Atómico Bariloche and Instituto Balseiro, Comisión Nacional de Energía Atómica, Bariloche R8402AGP, Argentina; fosco@cab.cnea.gov.ar

² Departamento de Física Juan José Giambiagi, FCEyN UBA, Facultad de Ciencias Exactas y Naturales, Ciudad Universitaria, Pabellón I, Buenos Aires 1428, Argentina; lombardo@df.uba.ar

* Correspondence: fdmazzi@cab.cnea.gov.ar

Abstract: We study the motion-induced radiation due to the non-relativistic motion of an atom, coupled to the vacuum electromagnetic field by an electric dipole term, in the presence of a static graphene plate. After computing the probability of emission for an accelerated atom in empty space, we evaluate the corrections due to the presence of the plate. We show that the effect of the plate is to increase the probability of emission when the atom is near the plate and oscillates along a direction perpendicular to it. On the contrary, for parallel oscillations, there is a suppression. We also evaluate the quantum friction on an atom moving at constant velocity parallel to the plate. We show that there is a threshold for quantum friction: friction occurs only when the velocity of the atom is larger than the Fermi velocity of the electrons in graphene.

Keywords: dynamical Casimir effect; quantum friction; graphene



check for updates

Citation: Fosco, C.D.; Lombardo, F.C.; Mazzitelli, F.D. Motion-Induced Radiation Due to an Atom in the Presence of a Graphene Plane. *Universe* **2021**, *7*, 158. <https://doi.org/10.3390/universe7050158>

Academic Editor: Galina L. Klimchitskaya

Received: 15 April 2021

Accepted: 13 May 2021

Published: 20 May 2021

Publisher's Note: MDPI stays neutral with regard to jurisdictional claims in published maps and institutional affiliations.



Copyright: © 2021 by the authors. Licensee MDPI, Basel, Switzerland. This article is an open access article distributed under the terms and conditions of the Creative Commons Attribution (CC BY) license (<https://creativecommons.org/licenses/by/4.0/>).

1. Introduction

Casimir and Casimir–Polder forces are physical manifestations of the vacuum fluctuations of the electromagnetic field which involve, respectively, the interaction between static bodies and between an atom and a body. The dependence of those effects on the geometry of the system, as well as on the electromagnetic properties of the material media and the atom, has been intensively investigated in the last decades, at both zero and nonzero temperatures [1–3].

Graphene, a single layer of carbon atoms, can be effectively described as a two-dimensional material. It owes its remarkable physical properties to its planar hexagonal crystal structure and to the fact that the electronic degrees of freedom can be described, at low energies, as Dirac fermions: indeed, they satisfy a linear dispersion relation, i.e., they behave as massless fermions that propagate with the Fermi velocity $v_F \simeq 0.003c$ [4]. This yields an unusual behavior for the conductivity, as well as peculiar transport and optical properties [5,6]. These features have understandably raised the interest in the analysis of the interaction of graphene with the vacuum electromagnetic field fluctuations [7].

In natural units, the response function of graphene is determined by two dimensionless quantities, v_F , and the fine structure constant. Therefore, in the simplest configuration of two planar graphene sheets separated by a distance d at zero temperature, simple dimensional analysis implies that the static Casimir force has the same distance dependence as for perfect conductors; namely, it is proportional to $1/d^4$ (the force is weaker than for ideal conductors). However, new interesting effects appear at finite temperature [8]. Besides, the phenomenology becomes richer when considering more realistic descriptions for graphene, for example by including a gap in the dispersion relation or a non-vanishing chemical potential [9,10].

From a theoretical standpoint, the system is often amenable to a full ab-initio description in the context of a continuum quantum field theory, treating the microscopic

degrees of freedom as Dirac fields in two dimensions [11]. For the alluded Casimir and Casimir–Polder forces, the results of this approach have been shown to be equivalent to the ones derived from Lifshitz theory [10].

When atoms or macroscopic bodies are set in motion, new phenomena may appear. Motion induced radiation, or dynamical Casimir effect (DCE), consists in the production of photons from the vacuum due to acceleration [12–15]. A related but somewhat different effect is quantum friction (QF), which manifests itself on objects with a constant relative sliding velocity. Its origin is in the excitation of microscopic degrees of freedom of the bodies, mediated by the electromagnetic field. This results in a contactless dissipative force [16–19]. The interplay between atomic motion and quantum vacuum fluctuations has been analyzed in different contexts [20–23].

The DCE has been investigated in different models and physical setups, starting from the simplest case of a one-dimensional field theory in a cavity with a moving boundary [24], then a single accelerated mirror [25], and more recent calculations which focus on resonant effects [12–15]. The microscopic origin of the DCE [26,27] can be traced back to photon emission processes in accelerated atoms: indeed, even when the oscillation frequency is not sufficient to excite the atom, the coupling to the quantum electromagnetic field allows for the emission of photon pairs. Production of photons out of the vacuum can also occur in situations where the electromagnetic properties of a media change with time [28,29]. A practical implementation of this, involving superconducting circuits, has led to the first experimental observation of the DCE [30].

QF has also been discussed in a variety of situations, most of them involving planar sheets or semi-spaces electromagnetically described in terms of their dielectric properties. Due to its short range and very small magnitude, QF has eluded detection so far. Despite this, there could be observable traces of this effect in the velocity dependence of corrections to the accumulated geometric phase of a neutral particle which moves with constant velocity in front of an imperfect mirror [31]. It has also been shown that QF could influence the coherences of a two-level atom [32]. Furthermore, an innovative experiment was designed to track traces of QF by measuring this corrections to the geometric phase [33]. This experimentally viable scheme can spark, we believe, hope for the detection of non-contact friction.

Within the previous context of quantum dissipative effects, in this paper, we study a particular system which consists of an (externally driven) atom which moves non-relativistically (with or without acceleration) in the presence of a planar, static graphene sheet. Both systems are coupled to the vacuum electromagnetic (EM) field, which mediates the correlation between the quantum fluctuations of the charged degrees of freedom, located in the atom and on the graphene sheet. The atom is coupled to the EM field through its electric dipole moment. Because of the special features of graphene, for example, the dependence of its response function on just two dimensionless parameters, we expect an interesting manifestation of microscopic (i.e., one of the bodies involved is an atom) DCE and QF.

In a previous work [34], we studied QF between two sliding graphene sheets and found that there was a velocity threshold for the occurrence of friction, given by the Fermi velocity v_F . This fact could be eventually relevant, in future technological applications, in order to avoid dissipative effects. Note, however, that by the same token it makes QF almost impossible to detect in that kind of system. As we show below, a similar threshold appears for the case of an atom moving with constant velocity over a graphene sheet; we note in passing that the threshold may be less difficult to overcome for the motion of a single atom than for the collective motion of a whole plate.

We also previously studied the microscopic DCE due to an atom, with an internal structure modelled by a quantum harmonic oscillator, coupled to a scalar field, in the presence of an imperfect mirror [27]. The internal degrees of freedom of the mirror were described in terms of a set of harmonic oscillators. We found an interesting effect when the mechanical frequency equals to the sum of the internal frequency of the atom and that of the microscopic oscillators, with regions of enhancement and suppression of the vacuum

persistence amplitude. This behavior is similar to that of spontaneous emission for an atom immersed into a dielectric [35,36]. We expect a rather different behavior in the presence of the graphene plate, due to the already mentioned absence of a parameter with dimensions in the response function.

Many tools can be used to study the existence and magnitude of dissipative phenomena in this context; among them is the imaginary part of the in-out effective action, related with the vacuum persistence amplitude, and obtained by integrating out the quantum degrees of freedom. This results in an imaginary part which is a functional of the trajectory of the atom, the object that we evaluate here.

This paper is organized as follows. In Section 2, we define the model at a microscopic level. Then, in Section 3, we integrate out the charged degrees of freedom, to obtain the effective action for the gauge field, which also depends functionally on the trajectory of the atom. Results for the remaining functional integral (i.e., over the gauge field) are presented in Section 4, in a perturbative approach. To first order, the imaginary part of the effective action gives the probability of emission of the atom oscillating in vacuum that, up to this order, and to the quadratic order in the oscillation amplitude, is non-vanishing only when the frequency of oscillation is larger than the frequency of the harmonic oscillator that describes the atom. At higher orders in the amplitude, the threshold is reduced.

The second-order contribution contains information about the influence of the presence of the graphene sheet on the empty space vacuum persistence amplitude. In Section 5, we present results about the imaginary part of the in-out effective action for different kinds of motion. We first consider the QF on an atom moving with constant velocity, parallel to the plane, and show that there is a threshold for QF. Then, we analyze the case of an oscillatory motion, perpendicular or parallel to the plane. We find that the effect of the plane on the emission probability depends crucially on the direction of motion. In Section 6, we comment on the changes in the expression for the effective action when the exact propagator for the gauge field in the presence of the graphene plane is used, and the way to implement the perfect conductor limit. Section 7 contains the conclusions of our work.

2. The Microscopic Model

We begin by defining the model in terms of its action \mathcal{S} , depending on the intervening degrees of freedom: A_μ , a 4-potential corresponding to the EM field, a Dirac field ψ , $\bar{\psi}$ in $2 + 1$ dimensions, for the electronic degrees of freedom on the graphene sheet, $\mathbf{r}(t)$, the center of mass of the atom, and $\mathbf{x}(t)$, the position of the electron (relative to that center of mass).

\mathcal{S} has the structure:

$$\mathcal{S} = \mathcal{S}(A; \mathbf{r}, \mathbf{x}; \bar{\psi}, \psi) = \mathcal{S}_0(A) + \mathcal{S}_g(\bar{\psi}, \psi; A) + \mathcal{S}_a(\mathbf{r}, \mathbf{x}; A), \tag{1}$$

where $\mathcal{S}_0(A)$ denotes the free EM action, while \mathcal{S}_g and \mathcal{S}_a are the graphene and atom actions, respectively, each including its coupling to the gauge field.

The free EM field action $\mathcal{S}_0(A)$, including a gauge fixing term, is given by

$$\mathcal{S}_0(A) = \int d^4x \left[-\frac{1}{4} F_{\mu\nu} F^{\mu\nu} - \frac{\lambda}{2} (\partial \cdot A)^2 \right], \tag{2}$$

with $F_{\mu\nu} = \partial_\mu A_\nu - \partial_\nu A_\mu$. Indices from the middle of the Greek alphabet (μ, ν, \dots) run from 0 to 3, with $x^0 \equiv ct$. In our conventions, $c \equiv 1$, and we use the metric signature $(+ - - -)$.

The graphene action, \mathcal{S}_g , on the other hand, is localized on the region occupied by the sheet which, in our choice of coordinates, corresponds to $x^3 = 0$. Fields restricted to such region will therefore depend on the reduced, $2 + 1$ -dimensional space-time coordinates (x^0, x^1, x^2) , which we denote collectively as $x_{||}$. For an unstrained plate, the form of the action for a single fermionic flavor becomes:

$$\mathcal{S}_g(\bar{\psi}, \psi; A) = \int d^3x \bar{\psi}(x_{||}) (i\rho_\beta^\alpha \gamma^\beta D_\alpha - m) \psi(x_{||}), \tag{3}$$

where $D_\alpha = \partial_\alpha + ieA_\alpha(x_{i1}, 0)$. Indices of the beginning of the Greek alphabet (α, β, \dots) run over the values 0, 1, and 2, and $(\rho_\beta^\alpha) = \text{diag}(1, v_F, v_F)$, with v_F the Fermi velocity. A single flavor corresponds to two 2-component spinors, and the representation chosen for the Dirac’s γ -matrices is such that parity is preserved even when the mass $m \neq 0$.

The atom, on the other hand, is described by a simplified model in which a single electron of charge e and mass m moves in the presence of a central potential V with origin at the nucleus, where most of the mass M of the atom, and a charge $-e$, are located.

The trajectory of the center of mass of the atom is practically identical to the one of the nucleus, and we describe it by the vector function $t \rightarrow \mathbf{r}(t)$. Denoting by $\mathbf{x}(t)$ the position of the electron with respect to the nucleus, the interaction action between the atom and the EM field is:

$$S_a^{(int)} = \int dt [e(\dot{\mathbf{r}}(t) + \dot{\mathbf{x}}(t)) \cdot \mathbf{A}(t, \mathbf{r}(t) + \mathbf{x}(t)) - e A_0(t, \mathbf{r}(t) + \mathbf{x}(t)) - e\dot{\mathbf{r}}(t) \cdot \mathbf{A}(t, \mathbf{r}(t)) + e A_0(t, \mathbf{r}(t))] . \tag{4}$$

In the dipole approximation, i.e., assuming the fields vary smoothly on the spatial region where the electron’s wavefunction is spatially concentrated, we expand the interaction action as

$$S_a^{(int)} \approx e \int dt [\dot{\mathbf{r}} \cdot (\mathbf{A}(t, \mathbf{r} + \mathbf{x}) - \mathbf{A}(t, \mathbf{r})) + \dot{\mathbf{x}} \cdot \mathbf{A}(t, \mathbf{r} + \mathbf{x}) - \mathbf{x} \cdot \nabla\phi(t, \mathbf{r})].$$

After making an integration by parts and also using that $|\dot{\mathbf{r}}| \ll |\dot{\mathbf{x}}|$, the last expression can be written as

$$S_a^{(int)} \approx \int dt [\mathbf{d}(t) \cdot \mathbf{E}(t, \mathbf{r}(t)) + \mathbf{m}(t) \cdot \mathbf{B}(t, \mathbf{r}(t))],$$

with \mathbf{d} the electric dipole moment $\mathbf{d}(t) = e\mathbf{x}(t)$ and \mathbf{m} the magnetic dipole $\mathbf{m} = e/2 (\mathbf{x}(t) \times \dot{\mathbf{x}}(t))$. Neglecting the magnetic dipole term, one gets $S_a^{(int)} \simeq S_a^{(dip)}$, where:

$$S_a^{(dip)} = \int dt \mathbf{d}(t) \cdot \mathbf{E}(t, \mathbf{r}(t)) . \tag{5}$$

The total action for the atom, S_a , consistent with the approximations above, is then:

$$S_a = \int dt \left[\frac{m}{2} \dot{\mathbf{x}}^2(t) - V(\mathbf{x}(t)) + \mathbf{d}(t) \cdot \mathbf{E}(t, \mathbf{r}(t)) \right] , \tag{6}$$

where we ignore kinetic and potential terms for \mathbf{r} , since its dynamics is externally determined.

3. Effective Action

The effective action $\Gamma[\mathbf{r}(t)]$ is obtained by functional integration of all the degrees of freedom, with Feynman’s $i\epsilon$ prescription implicitly assumed for all the integrals, since we are interested in the in-out effective action, namely [37],

$$e^{i\Gamma(\mathbf{r})} = \frac{\int \mathcal{D}A \mathcal{D}\bar{\psi} \mathcal{D}\psi \mathcal{D}\mathbf{x} e^{iS(A; \mathbf{r}, \mathbf{x}; \bar{\psi}, \psi)}}{\int \mathcal{D}A \mathcal{D}\bar{\psi} \mathcal{D}\psi \mathcal{D}\mathbf{x} e^{iS(A; \mathbf{r}_0, \mathbf{x}; \bar{\psi}, \psi)}} , \tag{7}$$

where \mathbf{r}_0 is some ‘reference’ trajectory. In most applications, we use a time-independent \mathbf{r}_0 . This is useful when considering a bounded motion, where it is natural to identify it with the time average of $\mathbf{r}(t)$.

We find it useful to decompose the integral into two successive steps,

$$e^{i\Gamma(\mathbf{r})} = \frac{\int \mathcal{D}A e^{iS_{\text{eff}}(A; \mathbf{r})}}{\int \mathcal{D}A e^{iS_{\text{eff}}(A; \mathbf{r}_0)}} , \quad e^{iS_{\text{eff}}(A; \mathbf{r})} = \int \mathcal{D}\bar{\psi} \mathcal{D}\psi \mathcal{D}\mathbf{x} e^{iS(A; \mathbf{r}, \mathbf{x}; \bar{\psi}, \psi)} \tag{8}$$

where $S_{\text{eff}}(A; \mathbf{r})$ is assumed to be defined modulo an irrelevant constant, which cancels out in Γ . It is convenient to set: $S_{\text{eff}}(A; \mathbf{r}) = S_0(A) + S_I(A; \mathbf{r})$ where we separate from $S_{\text{eff}}(A; \mathbf{r})$ the free EM field contribution from the one due to the charged sources.

Therefore, we now need to integrate the fermionic field and the electron trajectories. In general, neither of them can be performed exactly; thus, consistently with the assumptions mentioned above, we retain the terms up to order e^2 . Namely, both produce terms which are quadratic in A .

Let us find the explicit form of those terms. In an obvious notation:

$$S_I(A; \mathbf{r}) = S_I^{(a)}(A; \mathbf{r}) + S_I^{(g)}(A). \tag{9}$$

In order to find $S_I^{(a)}$, one needs to perform the functional integral

$$e^{iS_I^{(a)}(A; \mathbf{r})} = \mathcal{N} \int \mathcal{D}\mathbf{x} e^{i \int dt \left(\frac{m}{2} \dot{\mathbf{x}}^2(t) - V(\mathbf{x}(t)) + e\mathbf{x}(t) \cdot \mathbf{E}(t, \mathbf{r}(t)) \right)}, \tag{10}$$

which, as usual, is assumed to vanish in the noninteracting case, i.e. $S_I^{(a)}|_{e=0} = 0$. This can be achieved by a proper choice of the constant \mathcal{N} .

We recognize the structure of $S_I^{(a)}(A; \mathbf{r})$ in (10) as the generating functional of $\mathbf{x}(t)$ connected correlation functions, regarding $e\mathbf{E}$ as the external source. A contribution of n th order in a series expansion of $S_I^{(a)}$ in powers of e , is therefore determined by the corresponding n -leg connected correlation function of $\mathbf{x}(t)$, in the absence of any external source. In particular, to the second order in the source,

$$S_I^{(a)}(A; \mathbf{r}) = \frac{ie^2}{2} \int dt \int dt' E_i(t, \mathbf{r}(t)) \langle x_i(t)x_j(t') \rangle E_j(t', \mathbf{r}(t')), \tag{11}$$

where

$$\langle x_i(t)x_j(t') \rangle = \frac{\int \mathcal{D}\mathbf{x} x_i(t)x_j(t') e^{i \int dt \left(\frac{m}{2} \dot{\mathbf{x}}^2(t) - V(\mathbf{x}(t)) \right)}}{\int \mathcal{D}\mathbf{x} e^{i \int dt \left(\frac{m}{2} \dot{\mathbf{x}}^2(t) - V(\mathbf{x}(t)) \right)}}. \tag{12}$$

This correlation function, due to time-translation and rotational invariances, regardless of the specific form of V , may be written as follows:

$$\langle x_i(t)x_j(t') \rangle = \delta_{ij} \int \frac{dv}{2\pi} e^{-iv(t-t')} \tilde{\Delta}(v), \tag{13}$$

with the precise form of $\tilde{\Delta}_a(v)$ to be determined by the potential. For example, for a harmonic potential of frequency Ω , $V = \frac{m}{2}\Omega^2\mathbf{x}^2$, one has the exact result:

$$\tilde{\Delta}(v) \equiv \tilde{\Delta}_\Omega(v) = \frac{1}{m} \frac{i}{v^2 - \Omega^2 + i\epsilon}. \tag{14}$$

For a general potential it is interesting to note that, since $\langle x_i(t)x_j(t') \rangle$ is the (exact) Feynman propagator of the coordinate operator, we can always invoke the spectral decomposition theorem to write:

$$\tilde{\Delta}(v) = \frac{1}{m} \int_0^\infty d\omega^2 \rho(\omega^2) \frac{i}{v^2 - \omega^2 + i\epsilon} \equiv \int_0^\infty d\omega^2 \rho(\omega^2) \tilde{\Delta}_\omega(v). \tag{15}$$

Therefore, for a general potential V ,

$$S_I^{(a)}(A; \mathbf{r}) = \frac{ie^2}{2} \int_0^\infty d\omega^2 \rho(\omega^2) \int dt \int dt' E_i(t, \mathbf{r}(t)) \Delta_\omega(t-t') E_j(t', \mathbf{r}(t')), \tag{16}$$

where $\Delta_\omega(t)$ is the inverse Fourier transform of $\tilde{\Delta}_\omega(v)$.

It is noteworthy that we obtain qualitatively similar results, to the quadratic order in the charge, if we assume that atom is described by a two-level system. Indeed, to that order, we only need to know the correlation function:

$$\langle x_i(t)x_j(t') \rangle = \langle 0|T[\hat{x}_i(t)\hat{x}_j(t')]|0 \rangle, \tag{17}$$

where T denotes the time-ordered product and $|0\rangle$ is the ground state of the atom. If now we assume that we have a two-level system, we may produce a more explicit expression for the correlation function. Indeed, we may insert an identity operator I in the time-ordered product, written in terms of the two eigenstates of the atom’s Hamiltonian. One of those eigenstates is of course $|0\rangle$ with energy E_0 , and there is just one an excited level, $|1\rangle$. For a rotationally symmetric potential, the excited state must have a degeneracy consistent with the conservation of angular momentum. The simplest non-trivial one is 3. Therefore, we assume that the excited level has an energy E_1 , with the three degenerate eigenstates $|1^{(\alpha)}\rangle$, with $\alpha = 1, 2, 3$.

We then insert the identity written as: $I = |0\rangle\langle 0| + \sum_{\alpha=1}^3 |1^{(\alpha)}\rangle\langle 1^{(\alpha)}|$ into the time-ordered product of Heisenberg operators: $\hat{x}_i(t) = e^{it\hat{H}}\hat{x}_ie^{-it\hat{H}}$; it is important to note that Wigner–Eckart’s theorem implies that \hat{x}_i can only have non-vanishing matrix elements between the ground state and the excited ones. Thus,

$$\langle 0|T[\hat{x}_i(t)\hat{x}_j(t')]|0 \rangle = \theta(t - t') e^{-i(t-t')\Omega} \zeta_{ij} + \theta(t' - t) e^{-i(t'-t)\Omega} \zeta_{ji} \tag{18}$$

where $\Omega = E_1 - E_0$ and

$$\zeta_{ij} = \sum_{\alpha} \langle 0|\hat{x}_i|1^{(\alpha)}\rangle\langle 1^{(\alpha)}|\hat{x}_j|0 \rangle. \tag{19}$$

We see that ζ_{ij} behaves as a second-order tensor under rotations and, because of the rotational symmetry of the system, can only be proportional to δ_{ij} : $\zeta_{ij} = \chi^2 \delta_{ij}$, for some constant χ . Thus,

$$\begin{aligned} \langle x_i(t)x_j(t) \rangle &= (2\Omega \chi^2 m) \delta_{ij} \frac{1}{2m\Omega} [\theta(t - t') e^{-i(t-t')\Omega} + \theta(t' - t) e^{-i(t'-t)\Omega}] \\ &= (2\Omega \chi^2 m) \delta_{ij} \Delta_{\Omega}(t - t'). \end{aligned} \tag{20}$$

We conclude that, for this quadratic approximation to the effective action due to the atom, a two-level system produces essentially the same effect as a harmonic potential of frequency Ω , if $E_1 - E_0 \propto (2\chi^2 m)^{-1}$.

Regarding the graphene contribution, we see that:

$$\mathcal{S}_1^{(g)}(A) = \frac{1}{2} \int d^3x_{\parallel} \int d^3y_{\parallel} A^{\alpha}(x_{\parallel}, 0) \Pi_{\alpha\beta}(x_{\parallel}, y_{\parallel}) A^{\beta}(y_{\parallel}, 0), \tag{21}$$

with the tensor kernel $\Pi_{\alpha\beta}$ denoting the vacuum polarization tensor for the Dirac field on the plane.

Using a tilde to denote Fourier transformation, $\tilde{\Pi}_{\alpha\beta}$ may be decomposed into two irreducible tensors (projectors) adapted to the symmetries of the system. Introducing first the ingredients: $\check{k}^{\alpha} \equiv k^{\alpha} - k^0 n^{\alpha}$, $\check{g}_{\alpha\beta} \equiv g_{\alpha\beta} - n_{\alpha} n_{\beta}$ and $n^{\alpha} = (1, 0, 0)$, a convenient pair of projectors is $\mathcal{P}_{\alpha\beta}^l$ and $\mathcal{P}_{\alpha\beta}^t$, where

$$\mathcal{P}_{\alpha\beta}^t \equiv \check{g}_{\alpha\beta} - \frac{\check{k}_{\alpha}\check{k}_{\beta}}{\check{k}^2}, \quad \mathcal{P}_{\alpha\beta}^l \equiv \mathcal{P}_{\alpha\beta}^{\perp} - \mathcal{P}_{\alpha\beta}^t, \quad \mathcal{P}_{\alpha\beta}^{\perp} \equiv g_{\alpha\beta} - \frac{k_{\alpha}k_{\beta}}{k^2}. \tag{22}$$

The result, for the most relevant case of $m = 0$, is as follows:

$$\begin{aligned} \tilde{\Pi}_{\alpha\beta} &= \alpha_N \sqrt{v_F^2 \mathbf{k}_\parallel^2 - k_0^2} \left[\mathcal{P}_{\alpha\beta}^t + \frac{\mathbf{k}_\parallel^2 - k_0^2}{v_F^2 \mathbf{k}_\parallel^2 - k_0^2} \mathcal{P}_{\alpha\beta}^l \right] \\ &= \alpha_N \sqrt{\mathbf{k}_\parallel^2 - k_0^2} \left[\sqrt{\frac{v_F^2 \mathbf{k}_\parallel^2 - k_0^2}{\mathbf{k}_\parallel^2 - k_0^2}} \mathcal{P}_{\alpha\beta}^t + \sqrt{\frac{\mathbf{k}_\parallel^2 - k_0^2}{v_F^2 \mathbf{k}_\parallel^2 - k_0^2}} \mathcal{P}_{\alpha\beta}^l \right], \end{aligned} \tag{23}$$

where we introduced $\alpha_N \equiv \frac{e^2 N}{16}$, with N the number of 2-component Dirac fermion fields. We thus find the explicit form of the two terms into which \mathcal{S}_I may be decomposed.

It is worth noting that, assuming gauge, translation, and rotation invariances, one can generalize the previous expression to other planar media as follows:

$$\tilde{\Pi}_{\alpha\beta}(k_\parallel) = g_t(k_\parallel) \mathcal{P}_{\alpha\beta}^t + g_l(k_\parallel) \mathcal{P}_{\alpha\beta}^l, \tag{24}$$

where g_t and g_l are functions of k_0 and $|\mathbf{k}_\parallel|$.

4. Perturbative Expansion

We now consider the evaluation of the effective action, by proceeding to integrate the vacuum field, in a perturbative expansion approach.

$\Gamma[\mathbf{r}(t)]$ is given by:

$$e^{i\Gamma[\mathbf{r}(t)]} = \langle e^{i\mathcal{S}_I(A;\mathbf{r})} \rangle \tag{25}$$

with

$$\langle \dots \rangle \equiv \frac{\int \mathcal{D}A \dots e^{i\mathcal{S}_0(A)}}{\int \mathcal{D}A e^{i\mathcal{S}_0(A)}}. \tag{26}$$

Γ may be expanded in powers of \mathcal{S}_{int} , producing a series of terms, namely, $\Gamma = \Gamma_1 + \Gamma_2 + \dots$. Let us consider the first two of them:

4.1. First-Order Contribution

We see that the first-order contribution, Γ_1 , contains two terms,

$$\Gamma_1 = \Gamma_1^{(a)} + \Gamma_1^{(g)}, \tag{27}$$

with

$$\Gamma_1^{(a,g)} = \langle \mathcal{S}_I^{(a,g)}(A;\mathbf{r}) \rangle. \tag{28}$$

It is clear that $\Gamma_1^{(g)}$ corresponds to a vacuum energy contribution, which is a well-known result for graphene.

We now consider $\Gamma_1^{(a)}$. We see that:

$$\Gamma_1^{(a)} = \frac{i}{2} e^2 \int dt \int dt' \Delta_\Omega(t-t') \langle \mathbf{E}(t, \mathbf{r}(t)) \cdot \mathbf{E}(t', \mathbf{r}(t')) \rangle, \tag{29}$$

which involves the free electric field correlation function. This may be expressed as follows:

$$\begin{aligned} \langle E_i(t, \mathbf{x}) E_j(t', \mathbf{x}') \rangle &= i \delta_{ij} \delta(t-t') \delta(\mathbf{x} - \mathbf{x}') \\ &+ i \int \frac{d^4 k}{(2\pi)^4} e^{-ik \cdot (\mathbf{x} - \mathbf{x}')} \frac{\mathbf{k}^2 \delta_{ij} - k_i k_j}{k_0^2 - \mathbf{k}^2 + i\epsilon}. \end{aligned} \tag{30}$$

The first line in the electric-field correlation, when introduced in the effective action, induces a divergent energy shift. If l is a length characterizing the size of the atom, the energy shift reads $E_{div} = \frac{3e^2}{4m\Omega l^3}$.

Aside from this contribution, the second, finite one, may be conveniently studied in Fourier space, where it can be related to our previous results on the scalar model [27]. Introducing

$$f(\mathbf{p}, \nu) = \int_{-\infty}^{+\infty} dt e^{-i\mathbf{p}\cdot\mathbf{r}(t)} e^{i\nu t}, \tag{31}$$

the result for the finite part is,

$$\Gamma_1^{(a)} = \frac{1}{2} \int \frac{d\nu}{2\pi} \int \frac{d^3p}{(2\pi)^3} f(-\mathbf{p}, -\nu) f(\mathbf{p}, \nu) \Pi(\nu, \mathbf{p}), \tag{32}$$

where

$$\Pi(\nu, \mathbf{p}) \equiv -\frac{2ie^2}{m} \mathbf{p}^2 \int \frac{dp^0}{2\pi} \frac{1}{(p^0 - \nu)^2 - \Omega^2 + i\epsilon} \frac{1}{(p^0)^2 - \mathbf{p}^2 + i\epsilon}. \tag{33}$$

Therefore,

$$\text{Im}[\Gamma_1^{(a)}] = \frac{1}{2} \int \frac{d\nu}{2\pi} \int \frac{d^3p}{(2\pi)^3} |f(\mathbf{p}, \nu)|^2 \text{Im}[\Pi(\nu, |\mathbf{p}|)], \tag{34}$$

where

$$\text{Im}[\Pi(\nu, |\mathbf{p}|)] = \frac{\pi e^2 |\mathbf{p}|}{m\Omega} [\delta(\nu - |\mathbf{p}| - \Omega) + \delta(\nu + |\mathbf{p}| + \Omega)]. \tag{35}$$

From (35), we note that there is a threshold in the frequency ν , below which there is no photon emission. That is a threshold for a Fourier component of frequency ν in $f(\mathbf{p}, \nu)$, which is not necessarily the same as the frequency of motion, unless one expands the expressions in powers of the oscillation amplitudes. Indeed, recalling the definition of f , we see that for a small, bounded motion $\mathbf{r}(t) = \mathbf{r}_0 + \mathbf{y}(t)$, where \mathbf{r}_0 is the average position and $\mathbf{y}(t)$ the departure, a series expansion yields, up to the lowest non trivial order:

$$f(\mathbf{p}, \nu) = e^{-i\mathbf{p}\cdot\mathbf{r}_0} [2\pi \delta(\nu) - i\mathbf{p} \cdot \tilde{\mathbf{y}}(\nu)], \tag{36}$$

where $\tilde{\mathbf{y}}(\nu)$ is the Fourier transform of $\mathbf{y}(t)$. Since the time average of $\mathbf{y}(t)$ vanishes, $\tilde{\mathbf{y}}(0) = 0$. Upon insertion of this expansion for f into the imaginary part, we can integrate the spatial components of the momentum, to get, at the second order in the departure, the spectral form:

$$\text{Im}[\Gamma_1^{(a)}] = \frac{1}{2} \int \frac{d\nu}{2\pi} m^{ij}(\nu) \tilde{y}^i(-\nu) \tilde{y}^j(\nu), \tag{37}$$

where

$$m^{ij}(\nu) = \frac{e^2}{6\pi m\Omega} \delta^{ij} \theta(|\nu| - \Omega) (|\nu| - \Omega)^5. \tag{38}$$

Due to dimensional reasons, the spectrum has a different power law than that of the scalar counterpart of this model [27], as well as different coefficient and factor of 2 (due to the polarizations of the EM field).

In particular, for a small linear oscillatory motion with frequency ν_0 and amplitude \mathbf{s} , $\mathbf{y}(t) = \mathbf{s} \cos(\nu_0 t)$, we obtain a constant $\text{Im}[\Gamma_1^{(a)}]$ per unit time (vacuum decay rate):

$$\frac{\text{Im}[\Gamma_1^{(a)}]}{T} = \mathbf{s}^2 \frac{e^2}{24\pi m\Omega} \theta(|\nu_0| - \Omega) (|\nu_0| - \Omega)^5, \tag{39}$$

where T is the total time.

Thus far, this corresponds to the second order in the oscillation amplitude, always within the $\Gamma_1^{(a)}$ contribution. When considering the same oscillatory motion without expanding in powers of the amplitude, we note that f contains not just the oscillation frequency ν_0 but also its harmonics. Indeed, using the Jacobi–Anger expansion,

$$e^{-i\mathbf{p}\cdot\mathbf{r}(t)} = e^{-i\mathbf{p}\cdot\mathbf{s}\cos(v_0t)} = \sum_{n=-\infty}^{+\infty} (-i)^n J_n(\mathbf{p}\cdot\mathbf{s}) e^{-inv_0t} \tag{40}$$

(where J_n denotes a Bessel function of the first kind), we see that all the multiples of v_0 are going to be present in f , what means that the threshold Ω may be surpassed with a lower oscillation amplitude (if its amplitude is increased):

$$f(\mathbf{p}, \nu) = 2\pi \sum_{n=-\infty}^{+\infty} (-i)^n J_n(\mathbf{p}\cdot\mathbf{s}) \delta(\nu - nv_0) . \tag{41}$$

It is interesting to note that, if one considers oscillations involving more than one direction, for example when performing a circular motion, then the phenomenon above involves sums of the respective frequencies, since the expansion above produces a series for each factor.

For the single linear oscillation, we find:

$$\frac{\text{Im}[\Gamma_1^{(a)}]}{T} = \frac{e^2}{\pi m \Omega} \sum_{n=1}^{\infty} \left\{ \theta(nv_0 - \Omega) (nv_0 - \Omega)^3 \int_0^1 du J_n[(nv_0 - \Omega)|\mathbf{s}|u] \right\} . \tag{42}$$

A few comments are in order. On the one hand, the term quadratic in the oscillation amplitude is recovered if one assumes that v_0 is above the threshold, and one expands in powers of the amplitude each Bessel function. The $n = 1$ terms produces the term quadratic in the departure. On the other hand, if the oscillation frequency is lower than the threshold, one gets a contribution starting from $n > 1$. The relevance of the harmonics of the fundamental frequency in the DCE was previously pointed out for the case of semitransparent mirrors in [38].

4.2. Second Order

The second-order term is found to be given by:

$$\Gamma_2 = \frac{i}{2} \langle (\mathcal{S}_I - \langle \mathcal{S}_I \rangle)^2 \rangle = \Gamma_2^{(aa)} + \Gamma_2^{(gg)} + \Gamma_2^{(ag)} , \tag{43}$$

of which, in a self-explanatory notation, only the last one involves correlations between the atom and the graphene plate (the first one deals with the atom in free space, and the second one produces a contribution to the graphene self-energy):

$$\Gamma_2^{(ag)} = i \langle (\mathcal{S}_I^{(a)} - \langle \mathcal{S}_I^{(a)} \rangle) (\mathcal{S}_I^{(g)} - \langle \mathcal{S}_I^{(g)} \rangle) \rangle . \tag{44}$$

Introducing the explicit form of $\mathcal{S}_I^{(a)}$ and $\mathcal{S}_I^{(g)}$ and keeping the latter in terms of a yet unspecified vacuum polarization tensor, after some algebra, we get:

$$\Gamma_2^{(ag)} = \frac{1}{2} \int \frac{d^2\mathbf{k}_{\parallel}}{(2\pi)^2} \int \frac{dk_3}{2\pi} \int \frac{dp_3}{2\pi} \int \frac{d\nu}{2\pi} f(-\mathbf{k}_{\parallel}, k^3, -\nu) f(\mathbf{k}_{\parallel}, p^3, \nu) B(\nu, \mathbf{k}_{\parallel}, k^3, p^3) \tag{45}$$

where

$$B(\nu, \mathbf{k}_{\parallel}, k^3, p^3) = e^2 \int \frac{dk_0}{2\pi} \frac{\tilde{\Delta}_{\Omega}(k_0 + \nu) [\tilde{\Pi}_{ii}(k_{ii})k_0^2 + \tilde{\Pi}_{00}(k_{ii})(\mathbf{k}_{ii}^2 - k_3 p_3) - 2k_0 k_i \tilde{\Pi}_{0i}(k_{ii})]}{(k_0^2 - \mathbf{k}_{ii}^2 - k_3^2)(k_0^2 - \mathbf{k}_{\parallel}^2 - p_3^2)} . \tag{46}$$

In terms of the functions g_t and g_l ,

$$B(\nu, \mathbf{k}_{ii}, k^3, p^3) = -e^2 \int \frac{dk_0}{2\pi} \frac{\tilde{\Delta}_{\Omega}(k_0 + \nu) [k_0^2 g_t(k_{ii}) + k_{ii}^2 g_l(k_{ii}) - \frac{\mathbf{k}_{ii}^2}{k_{ii}^2} k_3 p_3 g_l(k_{ii})]}{(k_0^2 - \mathbf{k}_{ii}^2 - k_3^2)(k_0^2 - \mathbf{k}_{\parallel}^2 - p_3^2)} . \tag{47}$$

For the particular case of graphene, those functions may be conveniently represented by means of an integral representation:

$$\begin{aligned}
 g_t(k_{||}) &= 2\alpha_N (k_0^2 - v_F^2 \mathbf{k}_{||}^2) \int \frac{dq_3}{2\pi} \frac{1}{k_0^2 - v_F^2 \mathbf{k}_{||}^2 - q_3^2} \\
 g_l(k_{||}) &= 2\alpha_N (k_0^2 - \mathbf{k}_{||}^2) \int \frac{dq_3}{2\pi} \frac{1}{k_0^2 - v_F^2 \mathbf{k}_{||}^2 - q_3^2}, \tag{48}
 \end{aligned}$$

which, when used in (47), leads to:

$$\begin{aligned}
 B(v, \mathbf{k}_{||}, k^3, p^3) &= -2i \frac{e^2}{m} \alpha_N \int \frac{dq_3}{2\pi} \int \frac{dk_0}{2\pi} \frac{[k_0^2(k_0^2 - v_F^2 \mathbf{k}_{||}^2) + (k_{||}^2)^2 - \mathbf{k}_{||}^2 k_3 p_3]}{\times \frac{1}{((k_0+v)^2 - \Omega^2 + i\epsilon)(k_0^2 - \mathbf{k}_{||}^2 - k_3^2 + i\epsilon)(k_0^2 - \mathbf{k}_{||}^2 - p_3^2 + i\epsilon)(k_0^2 - v_F^2 \mathbf{k}_{||}^2 - q_3^2 + i\epsilon)}, \tag{49}
 \end{aligned}$$

where we wrote explicitly the $i\epsilon$ terms in the denominators. The next step is to integrate k_0 , which appears in a similar fashion as the momentum to integrate in a loop integral in a quantum field theory system, although in this case in 0 + 1 dimensions. This can be done in several ways, for example by the method of residues. After that integration, the imaginary part of B may be written as follows:

$$\begin{aligned}
 \text{Im} [B(v, \mathbf{k}_{||}, k^3, p^3)] &= \frac{\pi e^2 \alpha_N}{m\Omega} \int \frac{dq_3}{2\pi} \left\{ \begin{aligned} &\frac{(1-v_F^2)|\mathbf{k}_{||}|^4 + [(2-v_F^2)p_3^2 - p_3 k_3]|\mathbf{k}_{||}|^2 + 2p_3^4}{(p_3^2 - k_3^2) [(1-v_F^2)|\mathbf{k}_{||}|^2 + p_3^2 - q_3^2]} p \\ &+ \frac{(1-v_F^2)|\mathbf{k}_{||}|^4 + [(2-v_F^2)k_3^2 - k_3 p_3]|\mathbf{k}_{||}|^2 + 2k_3^4}{(k_3^2 - p_3^2) [(1-v_F^2)|\mathbf{k}_{||}|^2 + k_3^2 - q_3^2]} k \\ &+ \frac{(1-v_F^2)^2 |\mathbf{k}_{||}|^4 + [(-2 + 3v_F^2)q_3^2 - k_3 p_3]|\mathbf{k}_{||}|^2 + 2q_3^4}{[(1-v_F^2)|\mathbf{k}_{||}|^2 + k_3^2 - q_3^2] [(1-v_F^2)|\mathbf{k}_{||}|^2 + p_3^2 - q_3^2]} q \\ &\times [\delta(v - \Omega - p) + \delta(v + \Omega + p)] \\ &\times [\delta(v - \Omega - k) + \delta(v + \Omega + k)] \\ &\times [\delta(v - \Omega - q) + \delta(v + \Omega + q)] \end{aligned} \right\} \tag{50}
 \end{aligned}$$

where we introduced the shorthand notation: $p \equiv \sqrt{\mathbf{k}_{||}^2 + p_3^2}$, $k \equiv \sqrt{\mathbf{k}_{||}^2 + k_3^2}$, and $q \equiv \sqrt{v_F^2 \mathbf{k}_{||}^2 + q_3^2}$.

Note that the third term inside the integral can be integrated, by taking advantage of the δ -function involving q_3 .

Regarding the first and second terms, we see that they differ just in the interchange $k^3 \leftrightarrow p^3$, so we discuss just the first one: the sum of the two δ -functions may be replaced by the product: $\theta(|v| - \Omega) \delta(|v| - \Omega - p)$. Therefore, using the previous condition into the integral for the (only) factor involving q_3 ,

$$\begin{aligned}
 \int \frac{dq_3}{2\pi} \frac{1}{(1-v_F^2)|\mathbf{k}_{||}|^2 + p_3^2 - q_3^2} &= \int \frac{dq_3}{2\pi} \frac{1}{-v_F^2 |\mathbf{k}_{||}|^2 + (|v| - \Omega)^2 - q_3^2} \\
 &= -\theta(v_F |\mathbf{k}_{||}| - (|v| - \Omega)) \frac{1}{2\sqrt{v_F^2 |\mathbf{k}_{||}|^2 - (|v| - \Omega)^2}}, \tag{51}
 \end{aligned}$$

where the last equality follows from the use of a principal value prescription for the integral. Note however that the condition $p = |v| - \Omega$ forced by the δ -function implies that $v_F |\mathbf{k}_{||}| < |v| - \Omega$ for $v_F < 1$. Therefore, the first and second terms in Equation (50) do vanish.

Using this result, we see that the full imaginary part may be written as follows:

$$\begin{aligned}
 \text{Im} [B(v, \mathbf{k}_{||}, k^3, p^3)] &= \frac{\pi e^2 \alpha_N}{m\Omega} \theta(|v| - \Omega) \theta(|v| - \Omega - v_F |\mathbf{k}_{||}|) \\
 &\times \frac{[|\mathbf{k}_{||}|^4 - [(2 + v_F^2)(|v| - \Omega)^2 + k_3 p_3]|\mathbf{k}_{||}|^2 + 2(|v| - \Omega)^4]}{[|\mathbf{k}_{||}|^2 + k_3^2 - (|v| - \Omega)^2] [|\mathbf{k}_{||}|^2 + p_3^2 - (|v| - \Omega)^2] (|v| - \Omega)}. \tag{52}
 \end{aligned}$$

In what follows, we apply this result to the analysis of the dissipative effects on the motion of the atom induced by the presence of a graphene sheet.

5. Results

5.1. Quantum Friction

The first example that we consider corresponds to an atom moving with constant velocity \mathbf{u} , parallel the plane. A non-vanishing imaginary part of the effective action would indicate the presence of quantum friction produced by the graphene.

The trajectory of the atom is given by $\mathbf{r}(t) = (0, ut, a)$. From Equation (31), we obtain

$$f(\mathbf{k}, v) = 2\pi e^{-ik^3 a} \delta(v - k^1 u). \tag{53}$$

Therefore, denoting by T the total extent of the time interval, we see that the imaginary part of the effective action per unit time becomes:

$$\text{Im} \left[\frac{\Gamma_2^{(ag)}}{T} \right] = \frac{1}{2} \int \frac{dk^1}{2\pi} \frac{dk^2}{2\pi} \frac{dk^3}{2\pi} \frac{dp^3}{2\pi} e^{-i(p^3+k^3)a} \text{Im} \left[B(k^1 u, \mathbf{k}_\parallel, k^3, p^3) \right]. \tag{54}$$

We see that, due to the presence of the threshold in the imaginary part of B , there will not be friction for $u < v_F$.

Note, however, that $u > v_F$, there will be a non-vanishing imaginary part. The physical reason is that, for that velocity, the frequency involved ($k^1 u$) can excite physical Dirac fermions on the graphene sheet. Note also that, as the velocity of the atom is $u < 1$, the integrals over p^3 and k^3 are well-defined, since the denominator in Equation (52) never vanishes.

After integrating those variables, we get:

$$\begin{aligned} \text{Im} \left[\frac{\Gamma_2^{(ag)}}{T} \right] &= \frac{\pi e^2 \alpha_N}{8m\Omega} \int \frac{dk^1}{2\pi} \frac{dk^2}{2\pi} \theta[|k^1 u| - \Omega - v_F |\mathbf{k}_\parallel|] e^{-2a\sqrt{|\mathbf{k}_\parallel|^2 - (|k^1 u| - \Omega)^2}} \\ &\times \frac{2|\mathbf{k}_\parallel|^4 - (3 + v_F^2)(|k^1 u| - \Omega)^2 |\mathbf{k}_\parallel|^2 + 2(|k^1 u| - \Omega)^4}{[|\mathbf{k}_\parallel|^2 - (|k^1 u| - \Omega)^2] (|k^1 u| - \Omega)}. \end{aligned} \tag{55}$$

It is easy to verify that, under the assumptions mentioned above ($|\mathbf{k}_\parallel| > |k^1 u| - \Omega > v_F |\mathbf{k}_\parallel|$), the integrand is positive.

In Figure 1, we plot the imaginary part of the effective action as a function of the velocity of the atom. We see that, after the threshold and an initial plateau, quantum friction increases with the velocity. The results are qualitatively similar to those obtained for the quantum friction between graphene sheets in [34]. In that reference, the authors also showed how to obtain the frictional force from the imaginary part of the in-out effective action (54). Besides, the argument for the existence of a threshold presented in [34], for the case of two sliding graphene sheets, can be translated here in a rather direct way: consider the momentum and energy balance during a small time interval δt , assuming that both the frictional force and the dissipated energy are driven by pair creation. The only relevant component of the total momentum \mathbf{P} of the pair for the (momentum) balance is the one along the direction of the velocity v . Relating that component of \mathbf{P} to the frictional force, we see that:

$$F_{\text{fr}} \delta t = P_x. \tag{56}$$

On the other hand, the energy balance reads

$$F_{\text{fr}} v \delta t = \mathcal{E} \tag{57}$$

where \mathcal{E} is the energy of the pair. However, since the fermions are both on-shell, we have

$$\mathcal{E} \geq v_F |P_x| \tag{58}$$

(the equal sign corresponds to a pair with momentum along the direction of v). Dividing Equations (57) and (56), and taking into account Equation (58), we see that a necessary condition for friction to happen is $v \geq v_F$.

The situation considered here is more interesting for an eventual experimental observation of the effect, because frictional effects only exist if the speed of the sliding motion is larger than the Fermi velocity of the charge carriers in graphene, a condition that is more easily achieved for an atom than for a whole sheet (for example, for the implementation of the experimental proposal in [33]).

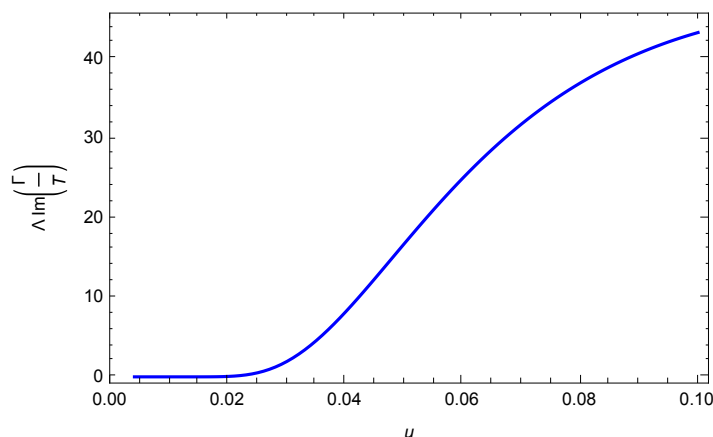


Figure 1. Imaginary part of the effective action as a function of the atom velocity u (dimensionless in natural units). There is no dissipative effect until $u > v_F = 0.003$, and QF increases as the parallel speed of the atom grows. We set $\Lambda = 8a^3 m\Omega / (\pi e^2 \alpha_N)$ and $\Gamma_2^{(ag)} = \Gamma$.

5.2. Small Departures Normal to the Graphene Plane

In Section 4.1, we computed the vacuum persistence amplitude for an atom oscillating in vacuum. The result to lowest order in the amplitude is given in Equation (39), and without expanding in the amplitude in Equation (42).

Here, we consider the corrections to the vacuum persistence amplitude induced by the presence of a graphene sheet. To this end, we evaluate the imaginary part of $\Gamma_2^{(ag)}$ in a situation where the atom undergoes a bounded motion, always in a direction normal to the graphene. Although the expression for the imaginary part is not perturbative in the amplitude of the atom’s motion, we find here the result to the lowest order in that amplitude.

We assume $\mathbf{r}(t) = \mathbf{r}_0 + \mathbf{y}(t)$, where the mean position of the atom is $\mathbf{r}_0 = (0, 0, a)$, with $a > 0$. The departure, on the other hand, is $\mathbf{y}(t) = (0, 0, y_{\perp}(t))$. We just need to insert the corresponding f for this situation in the general expression; to the order we want to work, it is sufficient to use:

$$f(\mathbf{k}, \nu) = e^{-ik^3 a} [2\pi\delta(\nu) - ik^3 y_{\perp}(t) + \dots]. \tag{59}$$

The resulting imaginary part may be arranged, in a similar fashion as in (37), as follows:

$$\text{Im}[\Gamma_2^{(ag)}] = \frac{1}{2} \int \frac{d\nu}{2\pi} m_{\perp}(\nu) |\tilde{y}_{\perp}(\nu)|^2, \tag{60}$$

where

$$m_{\perp}(\nu) = - \int \frac{d^2 \mathbf{k}_{\parallel}}{(2\pi)^2} \int \frac{dk^3}{2\pi} \int \frac{dp^3}{2\pi} k^3 p^3 e^{-i(k^3+p^3)a} \text{Im}[B(\nu, \mathbf{k}_{\parallel}, k^3, p^3)]. \tag{61}$$

Unlike the case of quantum friction described in the previous section, in the calculation of $m_{\perp}^{(A)}(v)$, the evaluation of the k^3 and p^3 integrals should be handled with care, using a principal value prescription. We include some details of the calculation in Appendix A. The result of performing the integrals allows us to write

$$m_{\perp}(v) = \frac{e^2 \alpha_N}{8m\Omega} \theta(|v| - \Omega) (|v| - \Omega)^5 \varphi(|v|a - \Omega a), \tag{62}$$

where $\varphi(x)$ is a dimensionless function (of a dimensionless variable), given by:

$$\begin{aligned} \varphi(x) = \int_0^{v_f^{-2}} d\rho & \left(1 - \frac{3 + v_F^2}{2} \rho + \rho^2 \right) \left[\cos(2x\sqrt{1-\rho})\theta(1-\rho) \right. \\ & \left. + e^{-2x\sqrt{\rho-1}}\theta(\rho-1) \right]. \end{aligned} \tag{63}$$

This integral can be computed analytically in terms of elementary functions. To do this, it is useful to perform the change of variables $y = \sqrt{|\rho - 1|}$. The explicit expression reads

$$\varphi(x) = \varphi_1(x) + \varphi_2(x), \tag{64}$$

where

$$\begin{aligned} \varphi_1(x) = \frac{1}{8x^6} & \left[-30 + (v_F^2 - 1)(2x^2 + 3)x^2 + 2x(- (3v_F^2 + 17)x^2 + 4x^4 + 30) \sin(2x) \right. \\ & \left. + (4(v_F^2 + 4)x^4 - 3(v_F^2 + 19)x^2 + 30) \cos(2x) \right], \end{aligned} \tag{65}$$

and

$$\begin{aligned} \varphi_2(x) = \frac{e^{-\frac{2\sqrt{1-v_F^2}x}{v_F}}}{8v_F^5 x^6} & \left[v_F^7 x^2 (3 - 4x^2) + v_F^5 (-10x^4 + 57x^2 - 30) + v_F^3 (34x^4 - 60x^2) \right. \\ & - 8\sqrt{1 - v_F^2} x^5 + 4\sqrt{1 - v_F^2} v_F^2 x^3 (3x^2 - 10) + 6\sqrt{1 - v_F^2} v_F^6 x^3 \\ & - 2\sqrt{1 - v_F^2} v_F^4 x (x^2 - 6) (2x^2 - 5) - 20v_F x^4 \left. \right] \\ & + \frac{1}{8x^6} (30 - (v_F^2 - 1)x^2 (2x^2 + 3)). \end{aligned} \tag{66}$$

Some properties of the function $\varphi(x)$ can be derived from its analytic expression. For instance, in the limit $x \rightarrow 0$, it tends to the large finite value $\varphi(0) \simeq 1/(3v_F^6)$, while, in the large x limit, $\varphi(x) \simeq x^{-1} \sin(2x)$.

In Figure 2, we plot the function φ as a function of $x = a(|v| - \Omega)$. As anticipated, it reaches large amplitudes at very small values of x , but then approaches zero, oscillating with a small amplitude, for large x . The behavior of $m_{\perp}(v)$ at extremely small distances a between the atom and the graphene sheet is determined by that of $x^5\varphi(x)$, as can be seen in Figure 3.

5.3. Small Departures Parallel to the Graphene Plane

We now consider oscillations of the atom that are parallel to the graphene sheet. The trajectory of the particle is now given by $\mathbf{r}(t) = \mathbf{r}_0 + \mathbf{y}(t)$, where, as above, $\mathbf{r}_0 = (0, 0, a)$, with $a > 0$. The departure from the mean position is $\mathbf{y}(t) = (\mathbf{y}_{\parallel}(t), 0)$ and the corresponding f function reads:

$$f(\mathbf{k}, v) = e^{-ik^3 a} [2\pi\delta(v) - i\mathbf{k}_{\parallel} \cdot \tilde{\mathbf{y}}_{\parallel}(v) + \dots]. \tag{67}$$

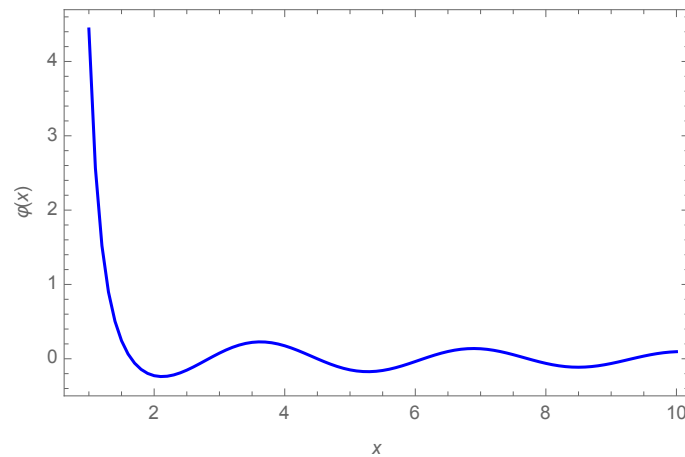


Figure 2. Dimensionless function φ as a function of $x = a(|\nu| - \Omega)$ (also dimensionless).

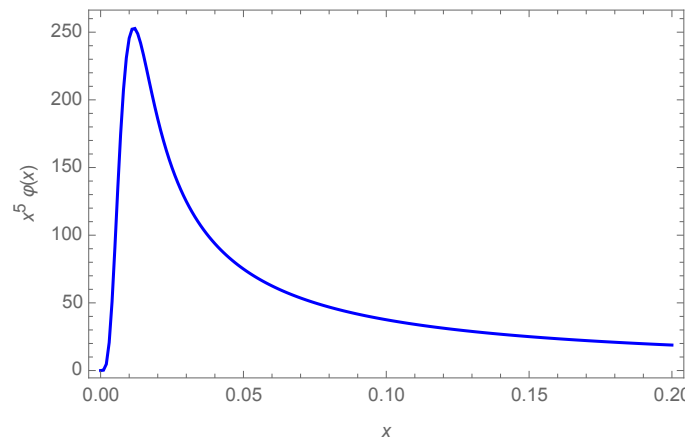


Figure 3. Small x behavior of the product $x^5\varphi(x)$.

The imaginary part of the effective action reads

$$\text{Im}[\Gamma_2^{(ag)}] = \frac{1}{2} \int \frac{d\nu}{2\pi} m_{\parallel}(\nu) |\tilde{\mathbf{y}}_{\parallel}(\nu)|^2, \tag{68}$$

where

$$m_{\parallel}(\nu) = \frac{1}{2} \int \frac{d^2\mathbf{k}_{\parallel}}{(2\pi)^2} \int \frac{dk^3}{2\pi} \int \frac{dp^3}{2\pi} |\mathbf{k}_{\parallel}|^2 e^{-i(k^3+p^3)a} \text{Im}[B(\nu, \mathbf{k}_{\parallel}, k^3, p^3)]. \tag{69}$$

The formal expression for $m_{\parallel}(\nu)$ is rather similar to that of $m_{\perp}(\nu)$, Equation (61), with the replacement $k^3 p^3 \rightarrow -1/2|\mathbf{k}_{\parallel}|^2$. Its evaluation proceeds along rather similar steps, and we therefore omit the details. The final result reads:

$$m_{\parallel}(\nu) = -\frac{e^2 \alpha_N}{16m\Omega} \theta(|\nu| - \Omega) (|\nu| - \Omega)^5 \phi(|\nu|a - \Omega a), \tag{70}$$

where

$$\begin{aligned} \phi(x) &= PV \int_0^{v_F^{-2}} d\rho \frac{\rho}{1-\rho} \left(\rho^2 - \frac{3+v_F^2}{2} \rho + 1 \right) \\ &\times [\cos(2x\sqrt{1-\rho})\theta(1-\rho) + e^{-2x\sqrt{\rho-1}}\theta(\rho-1)]. \end{aligned} \tag{71}$$

The integral that defines the function $\phi(x)$ has a singularity at $\rho = 1$. However, it is well defined with the principal value prescription.

We highlight the relation between this result and the function $\varphi(x)$ in Equation (63). Note that the difference is the extra factor $\rho/(1 - \rho)$ in the integrand of Equation (71). Therefore, we write

$$\begin{aligned} \phi(x) &= -\varphi(x) + PV \int_0^{v_F^{-2}} d\rho \left(\rho^2 - \frac{3+v_F^2}{2}\rho + 1\right) \times \frac{1}{1-\rho} \\ &\times [\cos(2x\sqrt{1-\rho})\theta(1-\rho) + e^{-2x\sqrt{\rho-1}}\theta(\rho-1)] \\ &\equiv -\varphi(x) + \chi(x). \end{aligned} \tag{72}$$

The function $\chi(x)$ can be computed analytically and can be written in terms of cosine integral and exponential integral functions. We omit this long expression here, but quote its main properties. For small values of x , we have $\chi(0) \simeq -1/(2v_F^4)$. This can be explicitly checked by setting $x = 0$ in the integral of Equation (72). On the other hand, for large values of x , it oscillates with an amplitude $O(x^{-1})$.

In Figures 4 and 5, we plot ϕ and $x^5\phi$ as functions of $x = a(|v| - \Omega)$. There is an important difference between the results for parallel and perpendicular motions. At short distances from the plane, in the case of parallel motion, the effect of the graphene is to decrease the probability of emission, while for perpendicular motion the probability is enhanced. Note that, at short distances, $|\chi(x)| \ll \varphi(x)$, and therefore $\phi(x) \simeq -\varphi(x)$, as clearly shown in Figures 3 and 5. On the other hand, at large distances, there is a partial cancellation between the $O(x^{-1})$ oscillations of $\varphi(x)$ and $\chi(x)$, and therefore $\phi(x)$ oscillates with a smaller amplitude, which is found to be of order $O(x^{-2})$.

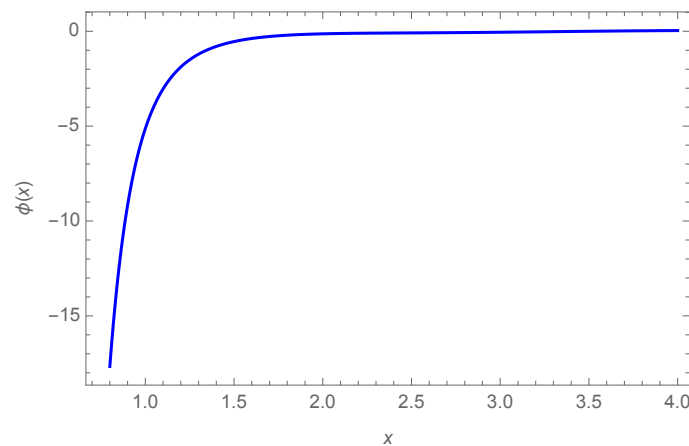


Figure 4. Dimensionless function ϕ as a function of $x = a(|v| - \Omega)$ (also dimensionless).

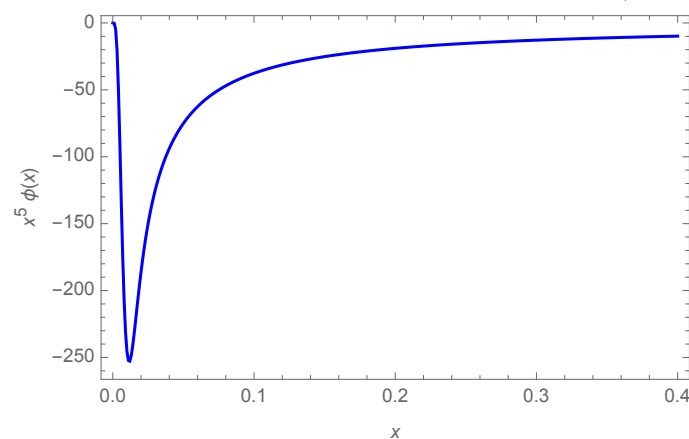


Figure 5. Small x behavior of the product $x^5\phi(x)$.

The fact that $m_{\parallel}(v)$ and $m_{\perp}(v)$ have different signs also occurs for a moving atom in front of a perfect conductor. In that case, the different signs come from the evaluation of the two-point functions using the image method.

6. The Exact Propagator for the Gauge Field in the Presence of the Sheet

In Section 4.2, we calculated the imaginary part of the effective action up to the first order in both $\mathcal{S}_I^{(a)}$ and $\mathcal{S}_I^{(g)}$. It is possible to derive an expression for the effective action which is of the first order in $\mathcal{S}_I^{(a)}$ and exact in $\mathcal{S}_I^{(g)}$. Indeed, one can for example sum over all the terms which appear when expanding the coupling to the sheet. Equivalently, one can calculate the exact gauge field propagator in the presence of the sheet and subtract the free propagator (which has already been considered).

Both approaches amount, at the level of the expression for B , to an identical expression as (47), but with different functions G_t and G_l replacing g_t and g_l , respectively, and defined as follows:

$$G_t = \frac{g_t}{1 + \frac{g_t}{2\sqrt{\mathbf{k}_\parallel^2 - k_0^2}}}, \quad G_l = \frac{g_l}{1 + \frac{g_l}{2\sqrt{\mathbf{k}_\parallel^2 - k_0^2}}}. \tag{73}$$

Therefore, it is possible to consider, within the same approach, some interesting phenomena. For example, we may take the limit $\alpha_N \rightarrow \infty$, under which both G_t and G_l tend to the same limit:

$$\alpha_N \rightarrow \infty \Rightarrow G_t, G_l \rightarrow 2\sqrt{\mathbf{k}_\parallel^2 - k_0^2}. \tag{74}$$

Recalling the functions g_t and g_l for graphene, we see that this limit can be treated by using the graphene expressions, but with $v_F = 1$ and $\alpha_N = 2$. In particular,

$$\begin{aligned} \text{Im} [B(\nu, \mathbf{k}_\parallel, k^3, p^3)] &= \frac{2\pi e^2}{m\Omega} \theta[|\nu| - \Omega - |\mathbf{k}_\parallel|] \\ &\times \frac{|\mathbf{k}_\parallel|^4 - [3(|\nu| - \Omega)^2 + k_3 p_3] |\mathbf{k}_\parallel|^2 + 2(|\nu| - \Omega)^4}{[|\mathbf{k}_\parallel|^2 + k_3^2 - (|\nu| - \Omega)^2] [|\mathbf{k}_\parallel|^2 + p_3^2 - (|\nu| - \Omega)^2] (|\nu| - \Omega)}, \end{aligned} \tag{75}$$

which is the kernel determining the dissipative effects in the case of an atom moving in front of a perfectly conducting plane. Of course, the velocity threshold means that now there will not be friction, since that would require the atom to move at superluminal speeds.

For intermediate values of α_N , we have:

$$\begin{aligned} G_t &= \alpha_N \frac{(\mathbf{k}_\parallel^2 - k_0^2) \sqrt{v_F^2 \mathbf{k}_\parallel^2 - k_0^2} - \frac{\alpha_N}{2} (v_F^2 \mathbf{k}_\parallel^2 - k_0^2) \sqrt{\mathbf{k}_\parallel^2 - k_0^2}}{(1 - (\frac{\alpha_N}{2})^2 v_F^2) \mathbf{k}_\parallel^2 - (1 - (\frac{\alpha_N}{2})^2) k_0^2} \\ G_l &= \alpha_N \frac{(\mathbf{k}_\parallel^2 - k_0^2) \sqrt{v_F^2 \mathbf{k}_\parallel^2 - k_0^2} - \frac{\alpha_N}{2} (\mathbf{k}_\parallel^2 - k_0^2) \sqrt{\mathbf{k}_\parallel^2 - k_0^2}}{(v_F^2 - (\frac{\alpha_N}{2})^2) \mathbf{k}_\parallel^2 - (1 - (\frac{\alpha_N}{2})^2) k_0^2}. \end{aligned} \tag{76}$$

This shows that, in the small α_N limit, we recover the singularities (cuts) on $k_0 = v_F |\mathbf{k}_\parallel|$ of the perturbative calculation. Note, however, that that contribution is overcome by the cut $k_0 = |\mathbf{k}_\parallel|$ for bigger values of α_N .

The effects that would result from considering the exact gauge field propagator (a resummation of the all terms involving a coupling to the medium) will, for graphene and other systems, be explored elsewhere.

7. Conclusions

We studied a model with an atom which moves non-relativistically, at both constant and non-constant speeds, in the presence of a planar graphene sheet. The model used for the atom is based on a dipole coupling which, as we showed, yields essentially the same results when one uses a harmonic coupling of the electron to the nucleus or when one instead implements a two-level description. This result appears when one considers the coupling of the atom to the EM field and integrates out the electron's degrees of freedom, to the lowest non-trivial order, which is quadratic in the electric field. Note that the order is exact in the harmonic case but approximate for a two-level system.

The quantum dissipative effects were studied by first deriving a general expression for a kernel which determines them (the imaginary part of the effective action) in terms of the motion of the atom. This general expression does not rely on the approximation

of small amplitude motion and therefore allows us to study both QF and the DCE on the same footing.

In the next step, we considered and evaluated the effects for particular states of motion: constant speed and bounded motion. For the former, we showed that QF exhibits the same threshold as for two graphene sheets moving at a constant relative speed [34]. It is interesting to remark that there is also a threshold in QF for non-dispersive dielectrics [39]. Indeed, when considering half-spaces described by a real constant dielectric function in relative motion, a frictional force arises between them when the velocity of moving half-spaces, in their center of mass frame, is larger than the phase speed of light in the medium (this is a quantum analog of the well-known classical Cherenkov radiation). In this respect, graphene behaves as a non-dispersive dielectric medium. For atoms moving near a metallic surface, although there is no threshold, QF is exponentially small at low velocities [40].

For bounded motion, we particularized to the case of oscillatory motions with small amplitudes along directions which are either normal or parallel to the sheet, at the second order in those amplitudes. Note that, at this order, the effects of those two motions superpose. We found that, in tune with the result for a moving atom near a perfect conductor, the effect of the graphene on the imaginary part of the effective action has different signs for normal and parallel motions.

We also pinpoint an effect mentioned above for when the atom moves in vacuum, but which is of more general validity: when the approximation of small amplitudes is not made for a simple harmonic motion, the system receives excitations of not only the fundamental frequency but also from its harmonics (of course with decreasing amplitudes); remember that the position of the atom appears in the exponent of a Fourier integral.

Author Contributions: The authors contributed equally to this work. All authors have read and agreed to the published version of the manuscript.

Funding: This research was supported by Agencia Nacional de Promoción Científica y Tecnológica (ANPCyT), Consejo Nacional de Investigaciones Científicas y Técnicas (CONICET), Universidad de Buenos Aires (UBA) and Universidad Nacional de Cuyo (UNCuyo). F.C.L. acknowledges the International Centre for Theoretical Physics and the Simons Associate Programme.

Conflicts of Interest: The authors declare no conflict of interest.

Appendix A. Evaluation of Principal Values

In the evaluation of $m_{\perp}(v)$ presented in Section 5.2, it is necessary to compute integrals of the form

$$I_{\pm}(n) = PV \int \frac{dk^3}{2\pi} \int \frac{dp^3}{2\pi} \frac{e^{-ia(k^3+p^3)} (k_3 p_3)^n}{(k_3^2 \pm A^2)(p_3^2 \pm A^2)}, \tag{A1}$$

where $A^2 = |\mathbf{k}_{\parallel}|^2 - (|v| - \Omega)^2$ and $n = 1, 2$. It is also useful to consider the case $n = 0$.

The computation of $I_{+}(n)$ is straightforward and gives

$$\begin{aligned} I_{+}(0) &= \frac{1}{4A^2} e^{-2Aa} \\ I_{+}(1) &= -\frac{1}{4} e^{-2Aa} \\ I_{+}(2) &= \frac{A^2}{4} e^{-2Aa}. \end{aligned} \tag{A2}$$

The principal value prescription is of course unnecessary in this case.

There is a subtlety in the evaluation of $I_{-}(n)$. Although at first sight $I_{-}(n)$ is the product of two independent integrals, the principal value of the product differs from the product of the principal values [41]. We illustrate the correct procedure for the particular case $n = 0$. Using Feynman parametrization and shifting the integration variable $k^3 \rightarrow k^3 - p^3$, we have

$$I_{-}(0) = PV \int_0^1 dx \int \frac{dk^3}{2\pi} e^{-iak^3} \int \frac{dp^3}{2\pi} \frac{1}{p_3^2 + x(1-x)k_3^2 - A^2}. \tag{A3}$$

Now, we implement the principal value prescription as

$$I_-(0) = \text{Re} \left[\int_0^1 dx \int \frac{dk^3}{2\pi} e^{-iak^3} \int \frac{dp^3}{2\pi} \frac{1}{p_3^2 + x(1-x)k_3^2 - A^2 + i\epsilon} \right]. \quad (\text{A4})$$

The calculation is now standard and yields:

$$I_-(0) = -\frac{1}{4A^2} \cos(2Aa). \quad (\text{A5})$$

The integrals for $n = 1, 2$ can be computed using the following trick:

$$-\frac{dI_n(0)}{da^2} = PV \int \frac{dk^3}{2\pi} \int \frac{dp^3}{2\pi} \frac{e^{-ia(k^3+p^3)} (k_3^2 + p_3^2 + 2k_3p_3)}{(k_3^2 - A^2)(p_3^2 - A^2)}. \quad (\text{A6})$$

Writing

$$k_3^2 + p_3^2 + 2k_3p_3 = k_3^2 - A^2 + p_3^2 - A^2 + 2k_3p_3 + 2A^2, \quad (\text{A7})$$

one can easily see that only the last two terms in the integral are not vanishing for $a \neq 0$. Therefore,

$$-\frac{dI_n(0)}{da^2} = 2A^2 I_-(0) + 2I_-(1) \implies I_-(1) = A^2 I_-(0). \quad (\text{A8})$$

Using a similar argument that involves the fourth derivative of $I_-(0)$, one can show that

$$I_-(2) = A^4 I_-(0). \quad (\text{A9})$$

From these results, it is rather straightforward to obtain Equation (62) for $m_\perp(\nu)$.

References

1. Milonni, P.W. *The Quantum Vacuum*; Academic Press: San Diego, CA, USA, 1994.
2. Milton, K.A. *The Casimir Effect: Physical Manifestations of Zero-Point Energy*; World Scientific: River Edge, NJ, USA, 2001.
3. Bordag, M.; Klimchitskaya, G.L.; Mohideen, U.; Mostepanenko, V.M. *Advances in the Casimir Effect*; Oxford University Press: Oxford, UK, 2009.
4. Castro Neto, A.H.; Guinea, F.; Peres, N.M.R.; Novoselov, K.S.; Geim, A.K. The electronic properties of graphene. *Rev. Mod. Phys.* **2009**, *81*, 109. [[CrossRef](#)]
5. Kuzmenko, A.; Van Heumen, E.; Carbone, F.; Van Der Marel, D. Universal Optical Conductance of Graphite. *Phys. Rev. Lett.* **2008**, *100*, 117401. [[CrossRef](#)] [[PubMed](#)]
6. Nair, R.R.; Blake, P.; Grigorenko, A.N.; Novoselov, K.S.; Booth, T.J.; Stauber, T.; Peres, N.M.; Geim, A.K. Fine structure constant defines visual transparency of graphene. *Science* **2008**, *320*, 1308. [[CrossRef](#)] [[PubMed](#)]
7. Bordag, M.; Fialkovsky, I.V.; Gitman, D.M.; Vassilevich, D.V. Casimir interaction between a perfect conductor and graphene described by the Dirac model. *Phys. Rev. B* **2009**, *80*, 245406. [[CrossRef](#)]
8. Bimonte, G.; Klimchitskaya, G.L.; Mostepanenko, V.M. How to observe the giant thermal effect in the Casimir force for graphene systems. *Phys. Rev. A* **2017**, *96*, 012517. [[CrossRef](#)]
9. Bordag, M.; Fialkovskiy, I.V.; Vassilevich, D.V. Enhanced Casimir effect for doped graphene. *Phys. Rev. B* **2016**, *93*, 075414; Erratum in *Phys. Rev. B* **2017**, *95*, 119905. [[CrossRef](#)]
10. Klimchitskaya, G.L.; Mostepanenko, V.M. Casimir and Casimir-Polder Forces in Graphene Systems: Quantum Field Theoretical Description and Thermodynamics. *Universe* **2020**, *6*, 150. [[CrossRef](#)]
11. Bordag, M.; Klimchitskaya, G.L.; Mostepanenko, V.M.; Petrov, V.M. Quantum field theoretical description for the reflectivity of graphene. *Phys. Rev. D* **2015**, *91*, 045037; Erratum in *Phys. Rev. D* **2016**, *93*, 089907. [[CrossRef](#)]
12. Dodonov, V.V. Current status of the dynamical Casimir effect. *Phys. Scr.* **2010**, *82*, 038105. [[CrossRef](#)]
13. Dalvit, D.A.R.; Maia Neto, P.A.; Mazzitelli, F.D. Fluctuations, dissipation and the dynamical Casimir effect. *Lect. Notes Phys.* **2011**, *834*, 419–457.
14. Nation, P.D.; Johansson, J.R.; Blencowe, M.P.; Nori, F. Stimulating Uncertainty: Amplifying the Quantum Vacuum with Superconducting Circuits. *Rev. Mod. Phys.* **2012**, *84*, 1. [[CrossRef](#)]
15. Dodonov, V.V. Fifty Years of the Dynamical Casimir Effect. *Physics* **2020**, *2*, 67–104. [[CrossRef](#)]
16. Volokitin, A.; Persson, B.N. Near-field radiative heat transfer and non-contact friction. *Rev. Mod. Phys.* **2007**, *79*, 1291. [[CrossRef](#)]
17. Pendry, J. Shearing the vacuum—Quantum friction. *J. Phys. Cond. Matter* **1997**, *9*, 10301. [[CrossRef](#)]
18. Pendry, J. Quantum friction—Fact or Fiction? *New J. Phys.* **2010**, *12*, 033028. [[CrossRef](#)]

19. Hoye, S.; Brevik, I.; Milton, K.A. Casimir friction between polarizable particle and half-space with radiation damping at zero temperature. *J. Phys. A* **2015**, *48*, 365004. [[CrossRef](#)]
20. Scheel, S.; Buhmann, S.Y. Casimir-Polder forces on moving atoms. *Phys. Rev. A* **2009**, *80*, 042902. [[CrossRef](#)]
21. Scheel, S.; Buhmann, S.Y. Path decoherence of charged and neutral particles near surfaces. *Phys. Rev. A* **2010**, *85*, 030101. [[CrossRef](#)]
22. Impens, F.; Behunin, R.O.; Ttira, C.C.; Neto, P.A.M. Non-local double-path Casimir phase in atom interferometers. *Eur. Phys. Lett.* **2013**, *101*, 60006. [[CrossRef](#)]
23. Intravaia, F.; Mkrtchian, V.E.; Buhmann, S.Y.; Scheel, S.; Dalvit, D.A.; Henkel, C. Friction forces on atoms after acceleration. *J. Phys. Cond. Matter* **2015**, *27*, 214020. [[CrossRef](#)]
24. Moore, G.T. Quantum theory of the electromagnetic field in a variable-length one-dimensional cavity. *J. Math. Phys.* **1970**, *11*, 2679. [[CrossRef](#)]
25. Davies, P.C.W.; Fulling, S.A. Radiation from Moving Mirrors and from Black Holes. *Proc. R. Soc. Lond. A* **1977**, *356*, 237–257.
26. de Melo e Souza, R.; Impens, F.; Maia Neto, P.A. Microscopic dynamical Casimir effect. *Phys. Rev. A* **2018**, *97*, 032514. [[CrossRef](#)]
27. Fariás, M.B.; Fosco, C.D.; Lombardo, F.C.; Mazzitelli, F.D. Motion induced radiation and quantum friction for a moving atom. *Phys. Rev. D* **2019**, *100*, 036013. [[CrossRef](#)]
28. Yablonovitch, E. Accelerating reference frame for electromagnetic waves in a rapidly growing plasma: Unruh-Davies-Fulling-DeWitt radiation and the nonadiabatic Casimir effect. *Phys. Rev. Lett.* **1989**, *62*, 1742. [[CrossRef](#)] [[PubMed](#)]
29. Agnesi, A.; Braggio, C.; Bressi, G.; Carugno, G.; Della Valle, F.; Galeazzi, G.; Messineo, G.; Pirzio, F.; Reali, G.; Ruoso, G. MIR: An experiment for the measurement of the dynamical Casimir effect. *J. Phys. Conf. Ser.* **2009**, *161*, 012028. [[CrossRef](#)]
30. Wilson, C.M.; Johansson, G.; Pourkabirian, A.; Simoen, M.; Johansson, J.R.; Duty, T.; Nori, F.; Delsing, P. Observation of the dynamical Casimir effect in a superconducting circuit. *Nature* **2011**, *479*, 376. [[CrossRef](#)]
31. Fariás, M.B.; Lombardo, F.C.; Soba, A.; Villar, P.I.; Decca, R.S. Towards detecting traces of non-contact quantum friction in the corrections of the accumulated geometric phase. *NPJ Quantum Inf.* **2020**, *6*, 1–7. [[CrossRef](#)]
32. Viotti, L.; Lombardo, F.C.; Villar, P.I. Enhanced decoherence for a neutral particle sliding on a metallic surface in vacuum. *Phys. Rev. A* **2021**, *103*, 032809. [[CrossRef](#)]
33. Lombardo, F.C.; Decca, R.S.; Viotti, L.; Villar, P.I. Detectable Signature of Quantum Friction on a Sliding Particle in Vacuum. *Adv. Quantum Tech.* **2021**, *2000155*, 1–9.
34. Fariás, M.B.; Fosco, C.D.; Lombardo, F.C.; Mazzitelli, F.D. Quantum friction between graphene sheets. *Phys. Rev. D* **2017**, *95*, 065012 [[CrossRef](#)]
35. Barnett, S.M.; Huttner, B.; Loudon, R. Spontaneous emission in absorbing dielectric media. *Phys. Rev. Lett.* **1992**, *68*, 3698. [[CrossRef](#)] [[PubMed](#)]
36. Barnett S.M.; Huttner, B.; Loudon, R.; Matloob, M. Decay of excited atoms in absorbing dielectrics. *J. Phys. B At. Mol. Opt. Phys.* **1996**, *29*, 3763. [[CrossRef](#)]
37. Fosco, C.D.; Lombardo, F.C.; Mazzitelli, F.D. Quantum dissipative effects in moving mirrors: A Functional approach. *Phys. Rev. D* **2007**, *76*, 085007. [[CrossRef](#)]
38. Fosco, C.D.; Giraldo, A.; Mazzitelli, F.D. Dynamical Casimir effect for semitransparent mirrors. *Phys. Rev. D* **2017**, *96*, 045004. [[CrossRef](#)]
39. Maghrebi, M.F.; Golestanian, R.; Kardar, M. Quantum Cherenkov Radiation and Non-contact Friction. *Phys. Rev. A* **2013**, *88*, 042509. [[CrossRef](#)]
40. Intravaia, F.; Behunin, R.O.; Henkel, C.; Busch, K.; Dalvit, D.A.R. Non-Markovianity in atom-surface dispersion forces. *Phys. Rev. A* **2016**, *94*, 042114. [[CrossRef](#)]
41. Davies, K.T.R.; Glasser, M.L.; Protopescu, V.; Tabakin, F. The mathematics of principal value integrals and applications to nuclear physics, transport theory, and condensed matter physics. *Math. Models Methods Appl. Sci.* **1996**, *6*, 833. [[CrossRef](#)]